

## A 94-GHz Cloud Radar System on a NASA High-Altitude ER-2 Aircraft

LIHUA LI

*Goddard Earth Sciences and Technology Center, University of Maryland, Baltimore County, Baltimore, Maryland*

GERALD M. HEYMSFIELD AND PAUL E. RACETTE

*NASA Goddard Space Flight Center, Greenbelt, Maryland*

LIN TIAN

*Goddard Earth Sciences and Technology Center, University of Maryland, Baltimore County, Baltimore, Maryland*

ED ZENKER

*Science Systems and Applications, Inc., Greenbelt, Maryland*

(Manuscript received 16 October 2003, in final form 19 March 2004)

### ABSTRACT

The 94-GHz (W band) Cloud Radar System (CRS) has been developed and flown on a NASA ER-2 high-altitude (20 km) aircraft. The CRS is a fully coherent, polarimetric Doppler radar that is capable of detecting clouds and precipitation from the surface up to the aircraft altitude in the lower stratosphere. The radar is especially well suited for cirrus cloud studies because of its high sensitivity and fine spatial resolution. This paper describes the CRS motivation, instrument design, specifications, calibration, and preliminary data from NASA's Cirrus Regional Study of Tropical Anvils and Cirrus Layers–Florida Area Cirrus Experiment (CRYSTAL–FACE) field campaign. The unique combination of CRS with other sensors on the ER-2 provides an unprecedented opportunity to study cloud radiative effects on the global energy budget. CRS observations are being used to improve our knowledge of atmospheric scattering and attenuation characteristics at 94 GHz, and to provide datasets for algorithm implementation and validation for the upcoming NASA CloudSat mission that will use a 94-GHz spaceborne cloud radar to provide the first direct global survey of the vertical structure of cloud systems.

### 1. Introduction

Clouds are a key element in the global hydrological cycle, and they have a significant role in the earth's energy budget through its influence on radiation budgets. Climate model simulations have demonstrated the importance of clouds in moderating and forcing the global energy budget (Houghton et al. 1995; Stephens et al. 1990). Despite the crucial role of clouds in climate and the breadth of our current knowledge, there are still many unanswered details (Stephens et al. 2002). An improved understanding of the radiative impact of clouds on the climate system requires a comprehensive view of clouds that includes their physical dimensions, vertical and horizontal spatial distribution, detailed microphysical properties, and the dynamical processes pro-

ducing them. However, the lack of finescale cloud data is apparent in current climate model simulations (Houghton et al. 1995; Stephens et al. 1990).

Clouds have been studied with various remote sensing methodologies, and it is recognized that no single active or passive sensor (optical or microwave) can measure all radiatively important clouds. Millimeter-wave radars at W band have been used over the past decade to provide finescale cloud information. These radars offer significant advantages over lidars and lower-frequency radars (Lhermitte 1987; Mead et al. 1994; Sekelsky and McIntosh 1996; Clothiaux et al. 1995; Hogan and Illingworth 1999). The high scattering efficiency and short wavelengths at millimeter-wave frequencies provide high sensitivity for cloud detection, and enable construction of compact, low-power consumption radars for use in airborne (Pazmany et al. 1994; Sadowy et al. 1997; Racette et al. 2003) and spaceborne (Li et al. 1994; Stephens et al. 2002) applications. The National Aeronautics and Space Administration's CloudSat mission, with a 2005 launch date, will employ a 94-GHz

---

*Corresponding author address:* Lihua Li, NASA Goddard Space Flight Center, Code 912, Building 33, Room C426, Greenbelt, MD 20771.

E-mail: lihua@agnes.gsfc.nasa.gov

spaceborne radar to measure vertical distribution of clouds globally (Stephens et al. 2002). Also, the joint Japanese/European Earth Cloud, Aerosol and Radiation Explorer (EarthCARE) mission has proposed a spaceborne W-band cloud radar (European Space Agency 2001). Data provided by these spaceborne cloud radars will improve our cloud detection capabilities on a global scale.

The original motivation for a nadir-pointing cloud radar on the ER-2 was to fill a gap in the detection of a broad range of clouds with the existing active ER-2 sensors. The ER-2 Cloud Physics Lidar (CPL), which has flown for a number of years, is ideally suited for cirrus clouds because of its high sensitivity (McGill et al. 2002); however, lidars are subject to severe attenuation in thick cirrus and may not penetrate through multiple layer clouds. The ER-2 Doppler Radar (EDOP), a precipitation radar at 9.6 GHz, will penetrate the most intense thunderstorms without complete attenuation before reaching the surface, but it is generally not as sensitive to clouds (Heymsfield et al. 1996). A W-band cloud radar not only fills the gap between a lidar and precipitation radar, but the overlap between the measurements can be useful in multiwavelength microphysics retrievals.

There is also a significant advantage of taking measurements from high altitudes above essentially all clouds. High-altitude cirrus clouds are extremely important in producing a net warming of the climate system, and ground-based cloud radar and lidar systems must look up through a substantial portion of the atmosphere, which can result in significant attenuation of the signal if intervening cloud layers are present and/or the lower atmosphere is extremely moist. Not only does this attenuation degrade the sensitivity of an upward-looking ground-based cloud radar at high altitudes, but it also results in an uncertainty in the radar reflectivity measurements. Downward-looking 94-GHz radar observations of cirrus and other clouds are clearly advantageous over comparable ground-based radar measurements that have to deal with strong water vapor and oxygen absorption in the boundary layer. Since the ER-2 flies at 20 km above the surface, a downward-looking cloud radar would be in closer proximity to the high cirrus clouds, so the radar sensitivity would be higher than a ground-based cloud radar with the same system parameters due to the inversed range-squared dependence of minimum detectable reflectivity. This has been an important issue when studying cirrus anvils, for example.

The NASA 94-GHz (W band) Cloud Radar System (CRS) was initiated in the early 1990s to provide cloud profiling capability on the ER-2, but it was completed in 2002 for flight on the ER-2. Since there were several existing remote and passive sensors on the ER-2 [CPL, EDOP, the Conical Scanning Submillimeter wave Imaging Radiometer (CoSSIR), the Moderate Resolution Imaging Spectrometer (MODIS) Airborne Simulator

TABLE 1. CRS system specifications.

Frequency (GHz)	94.155
IF frequency (MHz)	59.86
Peak power (kW)	1.7
Duty cycle	0.01 max
PRF (kHz)	0.5–20
Pulse width ( $\mu$ s)	0.25–2.0
Transmit polarization	V or H
Receive polarization	V and H
Noise figure (dB)	10.0
Receiver bandwidth (MHz)	1, 2, 4
Antenna beamwidth ( $^{\circ}$ )	0.6 $\times$ 0.8 (Airborne) 0.3 (Ground based)
Antenna gain (dB)	46.4 (Airborne, measured) 55 (Ground based)
Sensitivity (dBZ <sub>e</sub> )*	–29 (Airborne, from flight data) –46.9 (Ground based)

\* At 10-km range, 150-m range resolution, and 1-s averaging.

(MAS; King et al. 1996), as well as other sensors], the CRS was an important addition for cloud studies. The ER-2 ensemble of instruments including the CRS provides the unprecedented capability of studying various properties of clouds. Having all these instruments side by side provides the opportunity to compare them and thus determine the limitations of each sensor for cloud remote sensing.

The CRS is a Doppler, polarimetric radar (Racette et al. 2003) developed for autonomous operation on the ER-2 and for ground-based operation. In this paper, we provide an overview of the CRS system in section 3, with emphasis on its specifications and design of its radio frequency (RF), intermediate frequency (IF), and digital receiver subsystems. Section 4 discusses CRS calibration, which is essential for quantitative use of the reflectivity data, and minimum detectable reflectivity (MDR), which is important for cloud detectability. Section 5 presents reflectivity and Doppler observations from the first CRS operational deployment during NASA's Cirrus Regional Study of Tropical Anvils and Cirrus Layers–Florida Area Cirrus Experiment (CRYSTAL–FACE) field campaign (Jensen et al. 2003, personal communication).

## 2. System overview

The design of the CRS involved a compromise in order to address the scientific requirements that demand high sensitivity and high spatial and temporal resolution, and hardware limitations imposed by the size, power, and weight constraints of the ER-2 platform. Brown et al. (1995) suggested that cloud radar should have an MDR of  $-30$  dBZ<sub>e</sub> (equivalent radar reflectivity) in order to detect 99% (92% in the Tropics) of radiatively significant clouds in midlatitudes. The design goal of CRS MDR at a 10-km range was  $-30$  dBZ<sub>e</sub> after postaveraging to reduce the noise. With the parameters shown in Table 1, the CRS system noise floor for using a 1-MHz receiver bandwidth is  $-106$  dBm. On the other

hand, CRS should also be able to measure strong returns from intense targets such as the ocean surface. For the ER-2 flight altitude of 20 km, the ocean surface return power level in the CRS receiver is  $\sim -40$  dBm. Therefore, a receiver dynamic range larger than 70 dB is required to observe both the strong and weak signals without receiver saturation. Depending on the particular scientific objective, the spatial and vertical resolution requirements for radar measurements of clouds are typically less than 1 km spatial and 100 m vertical. These resolutions may not be required for global satellite measurements, but they are highly desirable for process studies that occur during typical field campaigns. These requirements can be easily achieved for a 94-GHz radar transmitting a short RF pulse with an antenna aperture size of approximately 0.3 m.

The ER-2 is a single-pilot aircraft thus requiring that CRS operates completely unattended over a typical 8-h flight. The entire radar system must have the capability to operate in a “turnkey” mode with internal monitoring of any faults that may occur in the transmitter or data system, and the capability to reset the system automatically in the event that a recoverable system failure is detected. The pilot has only two switches and fault indicator lights available for each instrument. In addition, the ER-2 imposed other engineering challenges for the CRS, including harsh environmental operating conditions at the surface and during flight ( $-60^\circ$  to  $+50^\circ\text{C}$ , 40 to 1000 hPa), limitations on size and weight, large data rates and data storage, and large range-Doppler ambiguities. The CRS was initially designed to meet these airborne requirements, but it can also be operated as a ground-based instrument with a larger antenna and higher sensitivity. The following discussion will describe the implementation of these requirements.

### 3. The CRS subsystems

The CRS consists of four subsystems including a 1) the RF/IF subsystem with high-voltage power supply and control electronics; 2) the antenna; 3) the data system/digital receiver, which performs data acquisition, processing, and storage; and 4) the environmental enclosure. The parameters characterizing CRS performance are listed in Table 1. Because of the other existing instruments on the ER-2, the CRS was installed in the tail cone of an ER-2 “superpod” located in the mid-section of a wing. The layout of the CRS in this superpod is shown in Fig. 1. The RF/IF and antenna subsystems are mounted in the tail cone of the right ER-2 superpod. The radar beam is pointed to nadir through an opening in the tail cone of the pod, which is open to the ambient environment so as to eliminate transmission effects of a radome. The digital receiver/data system is located in the midbody of the superpod, which is maintained at  $\sim 340$ -hPa pressure and temperatures above  $0^\circ\text{C}$ . In the ground-based configuration, the CRS

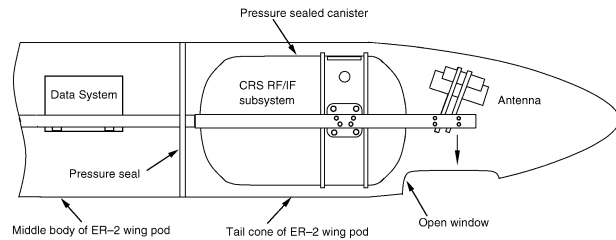


FIG. 1. CRS installation in ER-2 right wing pod. The CRS data system is installed in the pressurized middle body of the ER-2 wing pod, while the radar RF/IF subsystems and antenna are installed in the tail cone. The radar beam is pointed to nadir through an open window.

mounts on a mobile cart that has a two-axis gimballed positioner for scanning. A precision stepper motor controls the antenna elevation axis and enables range-height indicator (RHI) scanning with a higher-gain ground-based antenna. Figure 2 shows pictures of the ground-based and airborne CRS configurations.

#### a. RF/IF subsystems

Figure 3 shows a block diagram of the CRS. The custom-made RF subsystem, including the transmitter and RF receiver, was developed by former Pulse Technology, Inc., Marietta, Georgia, under the NASA Small Business Innovative Research (SBIR) program. It utilizes an Extended Interaction Amplifier (EIA; Communications and Power Industries, Canada) tube that transmits 1.7-kW peak power at 94 GHz. This subsystem also includes a novel power supply, EIA modulator, and timing control unit designed for ER-2 autonomous operation. The power supply uses three-phase 400-Hz power and includes active noise suppression.<sup>1</sup> The EIA modulator is capable of transmitting a wide variety of modulation schemes with range pulse widths between 0.25 and 3.0  $\mu\text{s}$  at pulse repetition frequencies (PRFs) up to 20 kHz (limited to 1% duty cycle), and with the capability to perform multiple PRFs. The transmit pulse timing can be generated internally using 32 preprogrammed PRF-pulse width pairs or from an external logic signal. The entire radar system is referenced to a shock-mounted ultrastable oscillator that generates five coherent frequencies. Among these five frequencies, the 9.976-MHz frequency from a crystal oscillator (phase noise at 10 kHz off from the center frequency is 175 dB down from the peak at the center frequency) serves as the phase reference to the other four. In the transmitter

<sup>1</sup> To achieve stability, a dual-loop high-voltage regulator is used. The first loop provides dc regulation to the EIA cathode with a linear regulator on the primary of the high-voltage transformers. The solid state, linear primary regulator circuit controls the peak 400-Hz three-phase voltage to the beam voltage rectifier in the high-voltage dc unit. A second loop uses a high-voltage capacitor to couple sense and error voltage to the cathode ac regulator at ground to reduce the ac ripple voltage on the EIA cathode.



FIG. 2. CRS hardware: (a) CRS setup in laboratory with the airborne antenna, (b) CRS data system installed in the middle body of ER-2 right wing pod, (c) CRS antenna and the canister housing the RF/IF subsystem installed in tail cone of ER-2 right wing pod, (d) CRS with the ground-based antenna mounted on the dual-axes gimbaled mobile cart.

chain, a phase-locked oscillator and six-time multiplier assembly generates the 94.155-GHz RF frequency and serves as the input of the transmitter. A second phase-locked oscillator and six-time multiplier assembly produces a signal that is 59.85 MHz lower than the RF signal and functions as the local oscillator signal for RF downconversion in the receiver. The network of latching circulators and isolators protects the receiver during the high-power pulse transmission and allows the switching of transmit polarization and simultaneous reception of co- and cross-polarization for the measurements of linear depolarization ratio (LDR) and differential reflectivity ( $Z_{DR}$ ). Following the switch network in the receiver chain is a mixer–amplifier assembly made by

Space Labs, Inc., California. This assembly has a single sideband noise figure of 7.5 dB. A noise diode is used as a calibrated source to monitor the gain and noise figure changes in the radar receivers. The average transmit power is monitored by a detector diode. Timing and control boards provide logic for the radar operation, monitor various fault conditions, and report these faults to the data system in the event of a system malfunction. All system status data, including fault conditions temperatures at the EIA and receiver hot points, voltage and current of the power supplies, etc., are multiplexed and sent to the data system for recording.

Ambient conditions of about  $-60^{\circ}\text{C}$  and 40-hPa pressure at the ER-2 cruising altitude required special con-

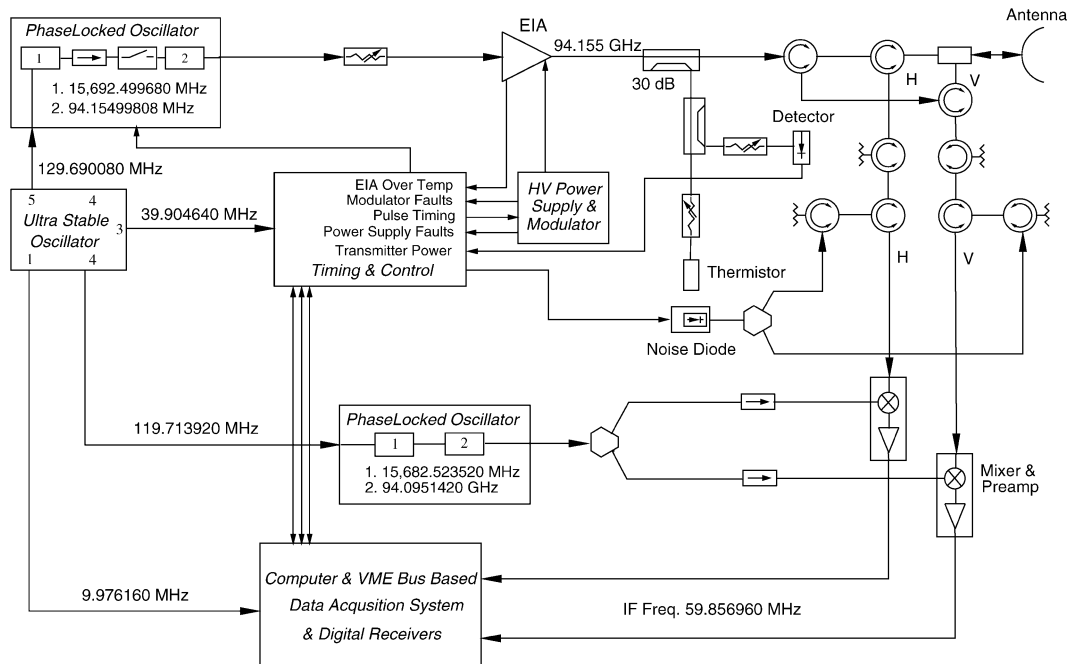


FIG. 3. Block diagram of 94-GHz CRS.

sideration in the development of the CRS. Under these conditions, failures will occur in the EIA transmitter, which uses high voltages ( $\sim 17$  kV) in the power supply/modulator and other electric components (e.g., electrolytic capacitors) normally operated at low altitudes. Therefore, the entire CRS RF/IF subsystem is housed in a pressure canister, which is sealed by a V-band clamp and can be easily opened for routine maintenance. During normal flight, the pressure canister maintains a constant pressure ( $\sim 1000$  hPa) at flight level, and a pressure relief valve is included as a safety feature to prevent implosion should the canister lose pressure during flight. Since the superpod has an open window to the environment, convective cooling caused by laminar airflow across this window results in significant heat loss through the wall of the canister. Heaters inside the canister and a NOMEX insulating blanket covering the outer body of the canister stabilize the instrument temperature during flight. The internal pressure and temperature of the vessel are constantly monitored. Should the pressure and temperature readings exceed the normal operation range, the radar will shut down automatically in order to protect key components.

The radar operates using one of two antennas (ground based or airborne) designed specifically for the CRS. Both antennas are novel designs utilizing Flat Parabolic Surface (FLAPS) technology and were developed by Malibu Research in Calabasas, California, under the NASA SBIR program. The ground-based Cassegrain antenna with a  $\sim 1$  m "square" aperture, has  $\sim 55$ -dBi gain and can fold up for storage to  $\sim 0.5$  m. The airborne antenna designed for installation on the ER-2 is an offset

parabolic reflector antenna with a pencil beam and 47-dBi gain. This antenna has two linearly polarized fixed-position feedhorns. The primary reflector is mounted to a two-axis gimbal with the capability to scan  $\pm 20^\circ$  across track and  $\pm 5^\circ$  along track for pitch correction. Motion control for automated positioning of the primary reflector is not yet implemented.

#### b. Digital receiver, data acquisition, and signal processing system

The data system is similar to the most recent implementation on the EDOP system (Heymsfield et al. 1996). It is based on the Versa Module Eurocard (VME) bus with a host computer that runs the VxWorks operating system and provides basic control and initialization of the system. Radar operation parameters can be modified through this host computer and preloaded into the data system before flight. The host computer also sends processed radar returns and aircraft navigation data to a 2.6-GB solid-state data recorder, which provides the improved reliability against vibration that is necessary for ER-2 operation.

The data system performs real-time processing from bandpass filtering of the IF signal to calculation of the interpulse covariance products. At the heart of the radar data system are the digital signal processing (DSP) boards designed by the National Center for Atmospheric Research (NCAR) in Boulder, Colorado. The NCAR boards include a digital receiver that ingests the 59.85-MHz IF signals from the radar RF receiver. Timing of the data processing is phase locked to the 9.96-MHz

stable reference from the radar RF/IF subsystem. The digital receiver has a 90-dB dynamic range that is achieved using two 12-bit analog-to-digital converters operating in parallel. Within the digital receiver, the IF is digitized into the in-phase (I) and quadrature (Q) signal components that are then match filtered. The data system also provides a timing signal for switching the transmit polarization for measurement of ZDR.

For Doppler processing on the ER-2, the range-Doppler ambiguity at 94 GHz necessitates using a dual-PRF (4 and 5 kHz) approach (Doviak and Zrnich 1993) to extend the unambiguous range and Nyquist interval. The 4-/5-kHz dual-PRF mode allows unambiguous Doppler measurements up to  $\pm 15.9 \text{ m s}^{-1}$  and an unambiguous range of 30 km. The Doppler processing is performed using an autocovariance estimator (pulse pair) on 720 gates. The integration time is programmable; for airborne operation the integration time is set to 0.5 s. The pulse-pair estimator greatly reduces the computational requirement over frequency domain (spectral) processing. The zeroth-, first-, and second-lag autocovariance products (real and imaginary components) for each gate are stored in the solid-state recorder; the mean Doppler and spectral width are estimated in postprocessing. In addition to the radar signal processing and status data, the data system captures low-rate (1 s) and high-rate (up to 64 Hz) aircraft attitude and navigation data from a Litton LTN-92 ring-laser inertial navigation system. The high-speed navigation data allow estimation of the aircraft motion corrections to Doppler velocities similar to that presented in Heymsfield et al. (1996). The first-order corrections are mainly due to pitch angle excursions and the vertical aircraft velocity. The latter quantity is estimated from integration of aircraft vertical velocity in a third-order feedback loop with GPS altitude. This provides vertical aircraft velocity estimates to better than  $0.5 \text{ m s}^{-1}$  in an absolute sense.

#### 4. System calibration and minimum detectable reflectivity

Radar calibration is an important issue for millimeter-wave cloud radars since errors in radar-reflectivity measurements have a direct impact on the retrieval of cloud microphysical properties. For instant, ice water content (IWC) can be estimated from radar reflectivity using an empirical relationship. If Brown et al.'s (1995) IWC versus radar-reflectivity relationship  $\text{IWC} = 0.153Z_e^{0.74}$  is used, then a 1-dB error in the radar reflectivity measurement will result in a 16% uncertainty in the IWC retrieval. However, the calibration of millimeter-wave radars is not simple (Li et al. 2001; Sekelsky 2002). The delicate nature of millimeter-wave components and the harsh environment in which they operate may cause undetected performance changes unless a regular system calibration is performed.

Millimeter-wave radar calibration is complicated by the difficulty in configuring the radar for calibration,

and the lack of absolute standards from which to establish calibration. To this end, we have applied different approaches to ensure the accuracy and stability of the CRS calibration. The CRS has an internal noise injection loop that monitors the gain and the front-end noise figure of the receivers. The average transmit power is continuously monitored through a diode detector and integration circuit. These measurements provide in-flight monitoring of the transmitter stability. In addition, the entire receiver path with the exception of the antenna was calibrated by injecting a W-band signal into the receiver port to provide an end-to-end (excluding the antenna) reference for the system. With measurements of the antenna gain and estimates of losses, the radar-system constant was estimated. However, uncertainties in losses and reflections of interconnected components require further consistency checks using external calibration measurements.

External calibration was performed using a trihedral corner reflector similar to that used for other W-band systems (Li et al. 2001; Sekelsky 2002). During this calibration, a 25.4-mm corner reflector was mounted on top of an 8-m-high, zenith-pointing pole tower. To reduce the clutter effect of the tower, the pole was made of low-reflection fiberglass and was further covered with absorbent materials. The tower was tilted a few degrees from zenith toward the radar in order to minimize speckle reflections. In addition to this target calibration, a radar intercomparison was performed at the University of Massachusetts (UMass), Amherst. The CRS was set up alongside the UMass ground-based Cloud Profiling Radar System (CPRS) 95-GHz cloud radar (Sekelsky and McIntosh 1996), which has been well maintained and calibrated over the past decade. Intercomparison measurements between the CRS and CPRS for similar cloud volumes were conducted during autumn 2002. During the 3-day intercomparison, both low-altitude stratus and midaltitude cirrus clouds were measured simultaneously by CPRS 95-GHz radar and CRS. Measurements were then compared for different cloud types and different collection times. The analyses demonstrated consistency between the two instruments to better than 1 dB. This result also agrees with the intercomparison between CRS and EDOP using measurements at cloud top, where the particle sizes are small and Rayleigh scattering is valid. EDOP has been well-calibrated from intercomparisons with the Tropical Rainfall Measuring Mission (TRMM) precipitation radar (PR), and from analysis of the ocean surface return (Heymsfield et al. 1996, 2000).

The ocean surface has been used to calibrate airborne and spaceborne radars (Meneghini and Kozu 1990; Durdan et al. 1994) and has been proposed as a calibration reference for CloudSat (Stephens et al. 2002). We have investigated the potential for using ocean surface scattering to validate CRS calibration (Li et al. 2003). In general, the scattering cross section,  $\sigma_0$ , is a function of radar frequency, radar beam incidence angle, and

ocean surface wind speed, as well as wind direction and polarization. During the calibration,  $\sigma_o$  was estimated using surface return at low incidence and quasi-specular scattering theory (Valenzuela 1978). It is worth noting that at 94 GHz, the attenuation caused by water vapor and oxygen absorption in the lower troposphere is significant (Clothiaux et al. 1995; Li et al. 2001). The data from CRYSTAL-FACE show that the averaged two-way integrated water vapor and oxygen absorption is about 5.8 dB with a standard deviation of 0.65 dB (Li et al. 2003). It is therefore necessary to correct this attenuation to ensure the accuracy of the  $\sigma_o$  estimate. This attenuation is calculated using meteorological data profiles, including temperature, pressure, and relative humidity obtained from ER-2-launched dropsondes and the Liebe (1985) millimeter-wave propagation model. Meanwhile, the dropsondes also provided measurements of near-surface wind conditions that are required to calculate  $\sigma_o$  using the quasi-specular scattering model. The analysis shows that the other CRS calibration results (i.e., using a corner reflector) agree with calculated  $\sigma_o$  to better than 1 dB as well.

The MDR of the CRS is estimated from the minimum detectable signal determined by the radar system noise level (Skolnik 1980). The mean noise power  $P_n$  is calculated using  $P_n = kT_oBF_n$ , where  $k$  is the Boltzman's constant,  $T_o$  is the reference temperature of 290 K, and  $F_n$  is the system noise figure. The CRS receiver noise figure including losses in the antenna, waveguide, and switch network is  $\sim 10$  dB. For a 1.0- $\mu$ s RF pulse (150-m range resolution) with a 1-MHz matched filter, the CRS single-pulse MDR at a 10-km range is  $-11.7$  dBZ<sub>e</sub> with the airborne antenna and  $-28.9$  dBZ<sub>e</sub> with the ground-based antenna. Noise averaging and noise subtraction is necessary to detect weak cloud signals. The typical CRS operation mode on the ER-2 is 4/5 kHz in the dual-PRF mode, resulting in an effective PRF of 4.444 kHz. For 1-s averaging and noise subtraction, the CRS MDR at a 10-km range is  $-29.7$  dBZ<sub>e</sub> with the airborne antenna. The actual MDR during CRYSTAL-FACE was  $-29$  dBZ<sub>e</sub> (150-m range resolution, 1-s time average). For ground-based operation, the corresponding MDR at a 10-km range is  $-46.9$  dBZ<sub>e</sub>. Figure 4 shows the CRS ground-based and ER-2 MDR for a 1-s averaging time and 1- $\mu$ s pulse width; the theoretical curve for 0.5- $\mu$ s pulse width is also shown. Note that for upper-tropospheric cirrus located at 15-km altitude (5 km from the radar), the MDR for the ER-2 is  $\sim -35$  dBZ<sub>e</sub> for the flight data.

## 5. CRS measurements from CRYSTAL-FACE

Tropical maritime thunderstorms are a significant producer of ice particles that are carried aloft and then exit into high-altitude anvils to be carried far from the generating thunderstorm. Quantifying the radiative, microphysical, and spatial properties of these thunderstorm-generated cirrus clouds and their evolution with time

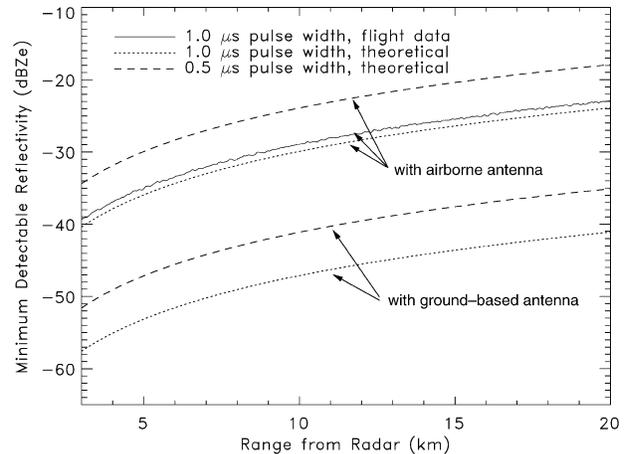


FIG. 4. CRS system MDR using 1-s averaging. The solid line shows the actual CRS minimum detectable reflectivity using 1.0- $\mu$ s pulse width during CRYSTAL-FACE.

was one of the key goals of the CRYSTAL-FACE campaign during July 2002 (more information available online at <http://cloud1.arc.nasa.gov/crystalface/>, also Jensen et al. 2003, personal communication). As one of the six aircraft operated during CRYSTAL-FACE, the ER-2 carried a full suite of sensors, including EDOP, CPL, CoSSIR, MAS, dropsondes, and other instruments. The ER-2 was based at Key West Naval Air Station, Florida, and conducted 11 scientific flights during the experiment. The CRS collected its first datasets from cirrus and thunderstorms, and it operated successfully during all the flights. In the following, we will show several data examples. Detailed analyses of combined CRS, EDOP, and CPL data from CRYSTAL-FACE will be discussed in separate papers (e.g., McGill et al. 2004).

On 9 July 2002, the ER-2 flew a "deep south" mission to remotely sense cirrus along with the WB-57 aircraft that sampled the tropical tropopause layer. The ER-2 flew to the south of the Gulf of Mexico through the Yucatan Channel, then flew across a thunderstorm-generated cirrus region off the east coast of Nicaragua and Honduras. Figure 5 shows CRS height-time sections of radar reflectivity (Fig. 5a) and Doppler velocity (Fig. 5b) for a flight leg between 1730 and 1748 UTC. The geographic coordinates of the start and end points are shown at the bottom of the plots. The CRS was able to penetrate through this thick cloud and light rain layer to detect the ocean surface. The ER-2 GPS altitude (nominally 20 km) was used to reference radar range to the surface, and the strong surface return is observed close to zero altitude, as expected. The measured Doppler velocities must be corrected for aircraft motions before they represent hydrometeor motions that are of scientific interest. In the absence of vertical air motions, these hydrometeor motions represent reflectivity-weighted hydrometeor fall speeds. The aircraft corrections are estimated using the ER-2 navigation information along with an estimate of the antenna tilt angle,

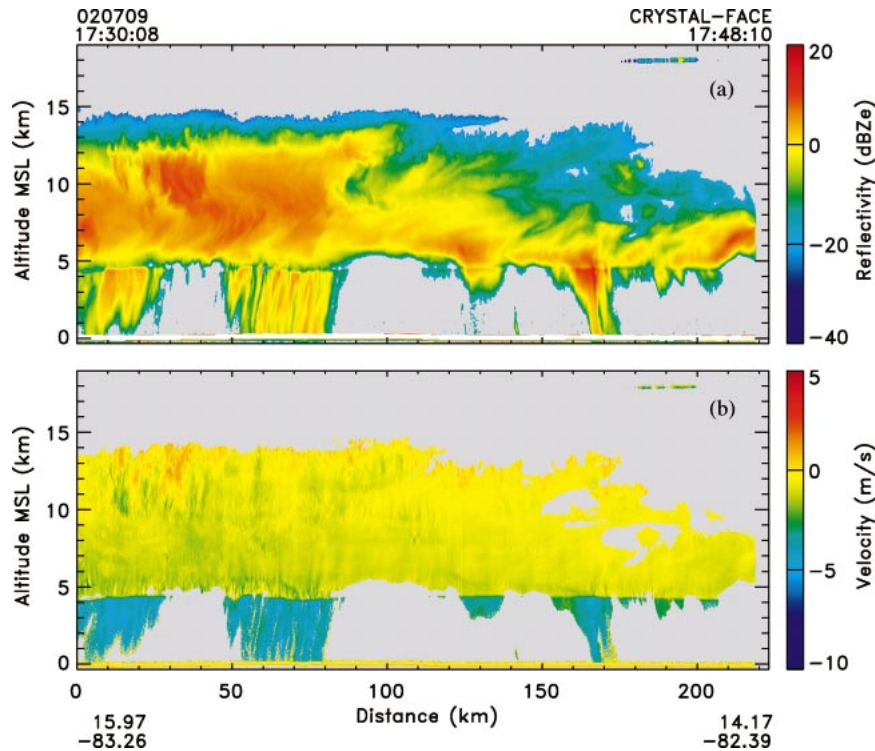


FIG. 5. CRS measurements on 7 Jul 2002 show ER-2 pass across thick anvil cirrus with light rain. (a) The equivalent radar reflectivity and (b) Doppler velocity corrected for aircraft motions (negative values are downward). The strong signal at zero altitude is the ocean surface return.

that is, the angle offset of the antenna along track (Heymsfield et al. 1996). This tilt angle was obtained using the Doppler velocity of the ocean surface, which should be  $0 \text{ m s}^{-1}$  in a statistical sense. The tilt angle was adjusted during the first few flights of the experiment in order to reduce the tilt angle to less than  $1^\circ$  as an average during flight (the ER-2 varies pitch angle by about  $2^\circ$  during flight). The Doppler velocity data shown in Fig. 5 were corrected for aircraft motions using this estimated tilt angle. The standard deviation of the mean velocity is approximately  $0.5 \text{ m s}^{-1}$ , which is primarily due to the uncertainty of ER-2 vertical motion. The spectral widths of hydrometeor fall velocity after subtracting the broadening due to the ER-2 horizontal motion ( $\sim 0.8 \text{ m s}^{-1}$ ) are approximately  $0.4 \text{ m s}^{-1}$  in ice clouds above 4.4-km altitude and  $0.3\text{--}1.2 \text{ m s}^{-1}$  in precipitation region below 4.4 km.

Several interesting features are noted in Fig. 5 where CRS detected a thick (4.4–15-km altitude) deep ice-cloud layer with occasional light rain below it. The transition from snow to rain typical for stratiform rain is clearly evident in this pass. The melting layer is observed at 4.4-km altitude from the sharp increase in velocity toward the surface below this altitude and below the band of lower reflectivity. These lower-reflectivity bands are due to Mie scattering by the large melting snowflakes as they fall through the melting region. In order to improve reflectivity sensitivity at cloud top,

reflectivity data were postaveraged, noise subtracted, and thresholded by the minimum detectable power level. The Doppler velocities were not suitable for noise subtraction since they were estimated using autocorrelation products based on measurements of phase shifts between pulses. Therefore, the reflectivity image exhibits several decibels better detectability of weak cloud than the velocity image.

The second case (Fig. 6) shows CRS measurements from high-level thin cirrus clouds off the west coast of Florida on 16 July 2002 that were generated by a localized convective storm. The CRS reflectivity and velocity between 2242 and 2248 UTC indicate that the cirrus extends between about 8 and 13.5 km. The cloud top is at a 6.5-km range from the ER-2 where the CRS MDR is approximately  $-33 \text{ dBZ}_e$ . Therefore, the CRS is able to detect weak cloud signals as low as  $-33 \text{ dBZ}_e$  at this altitude, which is difficult to achieve using a zenith-pointing ground-based W-band radar.

On 29 July 2002, a convective anvil was generated along the west coast of Florida (Fig. 7), which produced more significant rain (cf. Fig. 5). Figure 7a shows the CRS reflectivity from 2044 to 2101 UTC. The cloud top was at  $\sim 14 \text{ km}$  above the surface, while the melting layer in the raining region was at  $\sim 4\text{-km}$  altitude. The CRS penetrated through the storm system and measured the ocean surface return most of the time during this flight line. However, its signal experienced almost com-

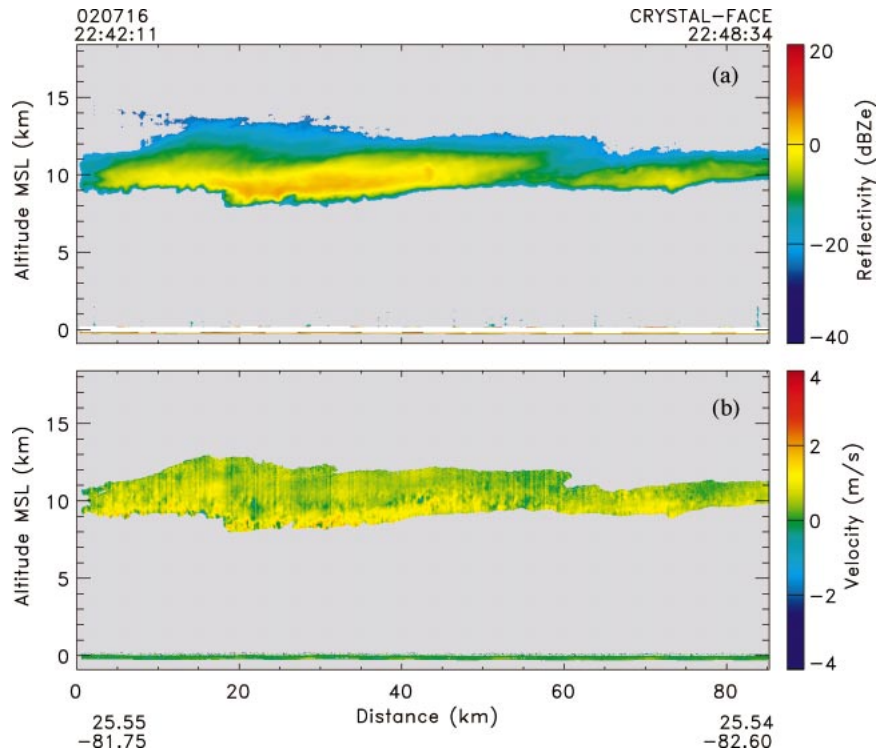


FIG. 6. Thin cirrus clouds near the west coast of south Florida on 16 Jul 2002 presented similarly as in Fig. 5.

plete attenuation in the region where it was raining (distance of  $\sim 125$  km or 2054 UTC). Figures 7b and 7c show the ocean surface reflectivity and the two-way path-integrated attenuation (PIA), respectively. For Fig. 7c, the ocean surface return from the rain-free and cloud-free region in the early part of this flight line is used as a reference to determine the PIA, which is a useful constraint for rain-rate and cloud microphysical property retrievals from airborne and spaceborne measurements (Meneghini et al. 1983). As is evident in Fig. 7c, the maximum PIA is over 36 dB, or about  $8 \text{ dB km}^{-1}$  when averaged over the 4-km rain path. A very rough estimate from Lhermitte (2002, his Fig. 4.10) indicates that this amount of attenuation is produced by a  $10 \text{ mm h}^{-1}$  rain rate. It is worth noting that the surface winds are likely different within and outside the precipitation regions. Also, the ocean surface roughness is likely different between rain and rain-free regions due to the wave damping effects of rain drops. Our current database of CRS ocean surface measurements with measured surface winds is quite limited because this was not a requirement in the first operational flights. Additional measurements will be made in future flights for studying the ocean surface scattering mechanism under different conditions.

## 6. Conclusions

The CRS provides an important new tool for studying clouds from a high-altitude, downward-looking vantage

point. It is capable of measuring most ice clouds and light rain through the troposphere and lower stratosphere. For cirrus cloud detection, the CRS has several unique advantages over ground-based millimeter-wave radars. First, because it operates in a downward-looking mode from a high-altitude platform, CRS measurements of the higher-altitude clouds are not affected by the water vapor and oxygen absorption, most of which is present at low altitudes. Second, radar sensitivity decreases with increasing range from the radar. Operating from on board the ER-2, the CRS is able to measure high-altitude cirrus clouds at a closer range than ground-based radars and upward-looking radars operated from mid- or low-altitude research aircrafts. Therefore, for some applications such as high-level cirrus measurements, the CRS has advantages over ground-based radars, even though these systems have larger antennas and somewhat higher sensitivity near the radar. Third, the CRS is able to use the ocean surface as a calibration reference to monitor system performance and to estimate total path attenuation, which is valuable for understanding the physics of W-band measurements and for cloud microphysical properties and rain-rate retrievals. CRS system calibration has been performed using different methods, including an external trihedral corner-reflector calibration, the ocean surface, and intercomparison with the UMass ground-based CPRS 95-GHz cloud radar. The results from all these methods agree within 1 dB.

The CRS collected its first airborne data from the

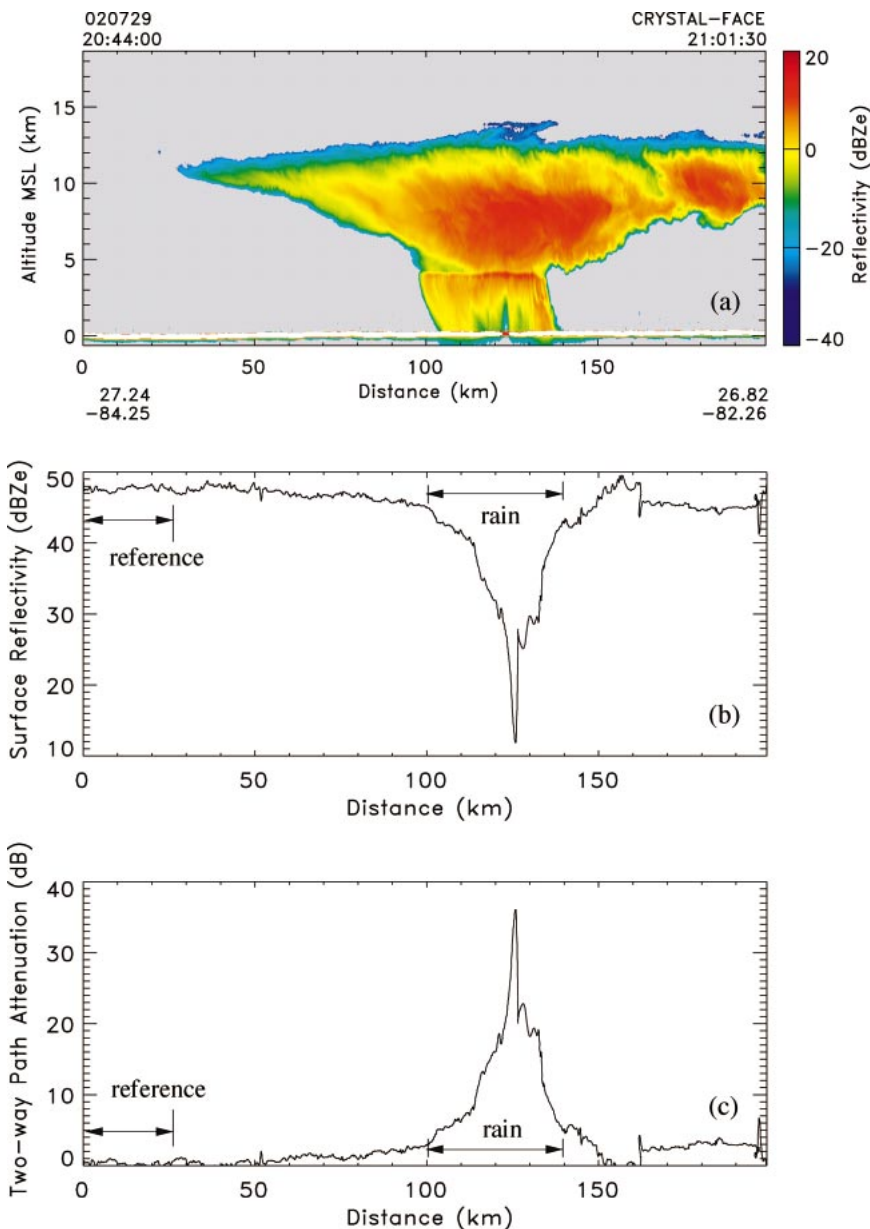


FIG. 7. Thick cirrus with moderate rain on 29 Jul 2002 off the west coast of south Florida: (a) equivalent radar reflectivity, (b) ocean surface reflectivity, and (c) two-way path-integrated attenuation estimated using surface reference technique.

CRYSTAL-FACE experiment during July 2002. It functioned exceptionally well during these flights, and ongoing data analyses have indicated that the extensive dataset collected will contribute toward meeting the scientific objectives of the experiments. The present emphasis is on further understanding W-band calibration using the ocean surface, and combining CRS, EDOP, CPL, and CoSSIR observations to improve cloud microphysical property retrievals.

*Acknowledgments.* Dr. Don Anderson of the NASA Atmospheric Radiation Program at NASA Headquarters

supported the CRS instrument completion and its participation in CRYSTAL-FACE. The CRS was a joint effort between the NASA Goddard Mesoscale Atmospheric Processes Branch, the Microwave Sensors Branch, and the Microwave Instrument Technology Branch. It has involved a variety of efforts that deserve special recognition. Dr. Steve Bidwell has contributed significantly to the development of the radar RF/IF and the data system. Mr. R. Aldridge has provided invaluable technical services for the radar. Thanks to Mr. Z. Zhang for his assistance on final RF/IF integration. Mr. Paul Weir is gratefully acknowledged for his design and

fabrication of the CRS canister and antenna-mounting structures. The CRS data-processing boards were obtained from NCAR, and Eric Loew is acknowledged for his help in implementing these boards. Former Pulse Technology of Marietta, Georgia, is appreciated for design and fabrication of the radar RF/IF subsystem and for technical support of the system tests. The NASA ER-2 crew is appreciated for support during the CRS installation, test flight, and field experiment. Dr. Jay Mace provided valuable scientific advice and support for CRS. Many other individuals helped in many varied ways.

## REFERENCES

- Brown, P. R., A. J. Illingworth, A. J. Heymsfield, G. M. McFarquhar, K. A. Browning, and M. Gosset, 1995: The role of spaceborne millimeter-wave radar in the global monitoring of ice clouds. *J. Appl. Meteor.*, **34**, 2346–2366.
- Clothiaux, E., M. Miller, B. Albrecht, T. Ackerman, J. Verlinde, D. Babb, R. Peters, and W. Syrett, 1995: An evaluation of a 94-GHz radar for radar remote sensing of cloud properties. *J. Atmos. Oceanic Technol.*, **12**, 201–229.
- Doviak, R. J., and D. S. Zrnic, 1993: *Doppler Radar and Weather Observations*. Academic Press, 562 pp.
- Durden, S. L., E. Im, F. K. Li, W. Ricketts, A. Tanner, and W. Wilson, 1994: ARMAR: An airborne rain-mapping radar. *J. Atmos. Oceanic Technol.*, **11**, 727–737.
- European Space Agency, 2001: EarthCARE—Earth clouds, aerosols and radiation explorer. Report for Assessment, The Five Candidate Earth Explorer Core Missions, SP-1257(1), ESA Publication Division, Noordwijk, Netherlands, 135 pp.
- Heymsfield, G. M., and Coauthors, 1996: The EDOP radar system on the high-altitude NASA ER-2 aircraft. *J. Atmos. Oceanic Technol.*, **13**, 795–809.
- , B. Geerts, and L. Tian, 2000: TRMM precipitation radar reflectivity profiles as compared with high-resolution airborne and ground-based radar measurements. *J. Appl. Meteor.*, **39**, 2080–2102.
- Hogan, R. J., and A. J. Illingworth, 1999: The potential of spaceborne dual-wavelength radar to make global measurements of cirrus clouds. *J. Atmos. Oceanic Technol.*, **16**, 518–531.
- Houghton, J. T., L. G. Meira Filho, B. A. Callander, N. Harris, A. Katenberg, and K. Maskell, 1995: *Climate Change 1995: The Science of Climate Change*. Cambridge University Press, 572 pp.
- King, M. D., and Coauthors, 1996: Airborne scanning spectrometer for remote sensing of clouds, aerosol, water vapor, and surface properties. *J. Atmos. Oceanic Technol.*, **13**, 777–794.
- Lhermitte, R. M., 1987: A 94-GHz Doppler radar for cloud observations. *J. Atmos. Oceanic Technol.*, **4**, 36–48.
- , 2002: *Centimeter and Millimeter Wavelength Radars in Meteorology*. Lhermitte Publications, 550 pp.
- Li, F., E. Im, S. Durden, and W. Wilson, 1994: Airborne and spaceborne cloud radar designs. *Proc. IGARSS 1994*, Pasadena, CA, IEEE, Vol. 2, 672–674.
- Li, L., and Coauthors, 2001: Retrieval of atmospheric attenuation using combined ground-based and airborne 95-GHz cloud radar measurements. *J. Atmos. Oceanic Technol.*, **18**, 1345–1353.
- , G. M. Heymsfield, P. E. Racette, and L. Tian, 2003: Calibration of a 94-GHz cloud radar using measurements from the ocean surface. Preprints, *31st Conf. on Radar Meteorology*, Seattle, WA, Amer. Meteor. Soc., 204–206.
- Liebe, H., 1985: An updated model for millimeter-wave propagation in moist air. *Radio Sci.*, **20**, 1069–1089.
- McGill, M., D. Hlavka, W. Hart, V. S. Scott, J. Spinhirne, and B. Schmid, 2002: Cloud physics lidar: Instrument description and initial measurements results. *Appl. Opt.*, **41**, 3725–3732.
- , and Coauthors, 2003: Combined lidar-radar remote sensing: Initial results from CRYSTAL-FACE. *J. Geophys. Res.*, **109**, D07203, doi: 10.1029/2003JD004030.
- Mead, J., A. Pazmany, S. Sekelsky, and R. McIntosh, 1994: Millimeter-wavelength radars for remotely sensing clouds and precipitation. *Proc. IEEE*, **82**, 1891–1906.
- Meneghini, R., and T. Kozu, 1990: *Spaceborne Weather Radar*. Arctech House, 199 pp.
- , J. Eckerman, and D. Atlas, 1983: Determination of rain rate from a spaceborne radar using measurements of total attenuation. *IEEE Trans. Geosci. Remote Sens.*, **21**, 34–43.
- Pazmany, A. L., R. E. McIntosh, R. Kelly, and G. Vali, 1994: An airborne 95-GHz dual polarization radar for cloud studies. *IEEE Trans. Geosci. Remote Sens.*, **1**, 731–739.
- Racette, P. E., G. M. Heymsfield, L. Li, L. Tian, and E. Zenker, 2003: The cloud radar system. Preprints, *31st Conf. on Radar Meteorology*, Seattle, WA, Amer. Meteor. Soc., 237–240.
- Sadowy, G., and Coauthors, 1997: The NASA DC-8 airborne cloud radar: Design and preliminary results. *Proc. IGARSS 1997*, Singapore, IEEE, Vol. 4, 1466–1469.
- Sekelsky, S. M., 2002: Near-field reflectivity and antenna boresight gain corrections for millimeter-wave atmospheric radars. *J. Atmos. Oceanic Technol.*, **19**, 468–477.
- , and R. E. McIntosh, 1996: Cloud observations with polarimetric 33 GHz and 95 GHz radar. *Meteor. Atmos. Phys.*, **59**, 123–140.
- Skolnik, M. I., 1980: *Introduction to Radar Systems*. McGraw Hill, 581 pp.
- Stephens, G. L., S. C. Tsay, P. W. Stackhouse, and P. J. Flatau, 1990: The relevance of the microphysical and radiative properties of cirrus clouds to climate and climate feedback. *J. Atmos. Sci.*, **47**, 1742–1752.
- , and Coauthors, 2002: The CloudSat mission and the A-train. *Bull. Amer. Meteor. Soc.*, **83**, 1771–1789.
- Valenzuela, G. R., 1978: Theories for the interaction of electromagnetic and oceanic waves—A review. *Bound.-Layer Meteor.*, **13**, 61–85.